



EARTH SCIENCES

Special Topic: Key Problems of the Deep Earth

Mineralogy of the deep lower mantle in the presence of H₂OHPSTAR
1100-2021Qingyang Hu ¹, Jin Liu ^{1,2,*}, Jiuhua Chen³, Bingmin Yan¹, Yue Meng⁴, Vitali B. Prakapenka⁵, Wendy L. Mao² and Ho-Kwang Mao^{1,*}¹Center for High Pressure Science and Technology Advanced Research (HPSTAR), Beijing 100094, China;²Department of Geological Sciences, Stanford University, Stanford, CA 94305, USA; ³Center for Study of Matter under Extreme Conditions, Department of Mechanical and Materials Engineering, Florida International University, Miami, FL 33199, USA; ⁴High Pressure Collaborative Access Team (HPCAT), X-ray ScienceDivision, Argonne National Laboratory, Argonne, IL 60439, USA and ⁵Center for Advanced Radiation Sources, University of Chicago, Chicago, IL 60437, USA

*Corresponding authors. E-mails: jin.liu@hpstar.ac.cn; maohk@hpstar.ac.cn

Received 21 April 2020; Revised 8 May 2020; Accepted 11 May 2020

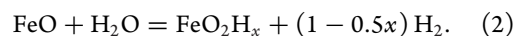
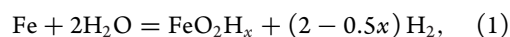
ABSTRACT

Understanding the mineralogy of the Earth's interior is a prerequisite for unravelling the evolution and dynamics of our planet. Here, we conducted high pressure-temperature experiments mimicking the conditions of the deep lower mantle (DLM, 1800–2890 km in depth) and observed surprising mineralogical transformations in the presence of water. Ferropicrinite, (Mg,Fe)O, which is the most abundant oxide mineral in Earth, reacts with H₂O to form a previously unknown (Mg,Fe)O₂H_x ($x \leq 1$) phase. The (Mg,Fe)O₂H_x has a pyrite structure and it coexists with the dominant silicate phases, bridgmanite and post-perovskite. Depending on Mg content and geotherm temperatures, the transformation may occur at 1800 km for (Mg_{0.6}Fe_{0.4})O or beyond 2300 km for (Mg_{0.7}Fe_{0.3})O. The (Mg,Fe)O₂H_x is an oxygen excess phase that stores an excessive amount of oxygen beyond the charge balance of maximum cation valences (Mg²⁺, Fe³⁺ and H⁺). This important phase has a number of far-reaching implications including extreme redox inhomogeneity, deep-oxygen reservoirs in the DLM and an internal source for modulating oxygen in the atmosphere.

Keywords: lower mantle, water-mantle interaction, ferropicrinite, high pressure, mantle mineralogy

INTRODUCTION

At depths of about 660–2890 km from the Earth's surface, the lower mantle represents the largest fraction of our planet (>55% by volume). In the lower mantle, the dominant upper-mantle ferromagnesian silicate mineral (Mg,Fe)₂SiO₄ breaks down into (Mg,Fe)O ferropicrinite (Fp) and (Mg,Fe)SiO₃ bridgmanite (Brg) [1,2], and this main mineral assemblage further transforms to Fp and post-perovskite (pPv) near the core-mantle boundary (CMB) [3,4]. Recent experiments revealed that the lower half of the deep lower mantle (DLM) beneath 1800 km in depth may be governed by remarkably different pressure-induced chemistry, leading to a set of unexpected mineralogical, geophysical and geochemical behaviors [5–7]. In the DLM, water becomes a strong oxidant that can oxidize iron [8] and common iron oxides [9] to form hydrogen-bearing FeO₂H_x ($x < 1$) with pyrite structure (Py) [10–12]:



However, pure iron and wüstite (FeO) are not major minerals in the lower mantle, and only become abundant when approaching the iron core; iron in the mantle is mostly present as an endmember component of ferromagnesian silicates or oxides. In the upper mantle and crust, Fe and Mg often form a complete solid solution in silicates, but in the lower mantle, they tend to be separated. Brg can only accommodate a maximum of 15 mole% Fe under the reducing DLM conditions, and the Fe-endmember silicate simply breaks down to simple oxides [13]. The key questions, therefore, are how much Mg can replace Fe to form (Mg, Fe)O₂H_x and under what *P-T* conditions? Here, we re-examined phase

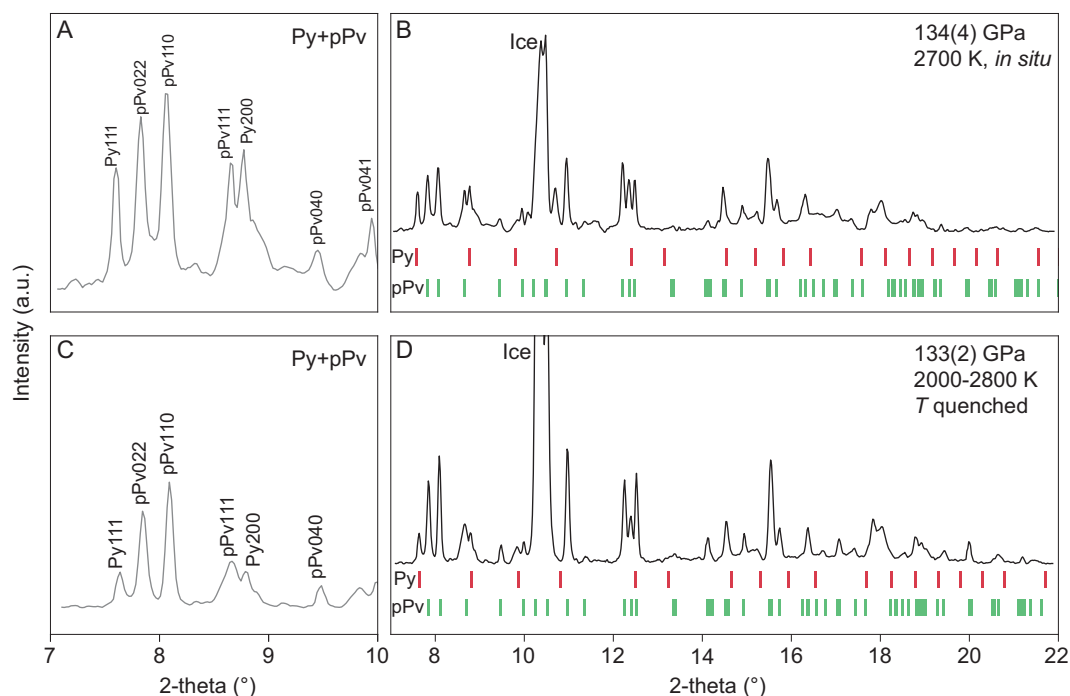


Figure 1. Py-phase synthesized from iron-bearing olivine (Fo80) and H₂O. (A, B) *In situ* XRD at 2700(100) K. New sets of diffraction peaks are associated with Py-phase and post-perovskite (Mg, Fe)SiO₃. (C, D) Quenched to RT. The X-ray wavelength was 0.3344 Å. (A, C) Zoomed in for signature high *d*-spacing peaks. Py, Py-phase; pPv, post-perovskite type (Mg, Fe)SiO₃.

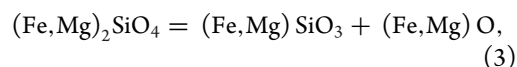
relations of ferromagnesian silicates and oxides in the presence of water and found very distinct mineralogy under the DLM conditions.

The polymorphic transition of olivine to wadsleyite at 410 km depth causes a seismic discontinuity that defines the top of the mantle transition zone (MTZ). With increasing depth (and pressure), wadsleyite transforms to ringwoodite and eventually decomposes to Fp plus Brg [2], causing the 660 km seismic discontinuity that defines the boundary between the MTZ and the lower mantle. Wadsleyite and ringwoodite can store 1–3 wt% water [14,15], which could make MTZ the largest water reservoir in the solid Earth. Schmandt *et al.* [16] explored the dehydration melting of hydrous peridotite at the top of the lower mantle, which may represent one of the key processes to transport water into the lower mantle [17–19]. Here, we further investigated the wadsleyite-water system down to the DLM, where dramatically different chemical behaviors lead to the creation of novel hydrous phases [20].

RESULTS

We performed high pressure-temperature (*P-T*) X-ray diffraction (XRD) experiments using laser-heated diamond anvil cells (DACs). A synthetic wadsleyite sample with composition (Mg_{0.8}Fe_{0.2})₂SiO₄ (Fo80) containing 2 wt%

water and an olivine sample with composition (Mg_{0.7}Fe_{0.3})₂SiO₄ (Fo70) were used as starting materials and loaded with water into the sample chambers of two DACs. Fo80 was compressed to 134 GPa and heated to 2800 K to mimic conditions of the CMB. The sample assemblage was probed *in situ* at high *P* using synchrotron XRD during laser heating (Fig. 1). Fo80 decomposed into pPv-type (Mg, Fe)SiO₃ and a pyrite-structured oxide phase (Mg, Fe)O₂H_x (Py-phase), instead of the well-known decomposition product of Fp in the anhydrous case. The Py-phase was quenchable to room temperature (RT) at high pressure (Fig. 1C and D). The Fo70 in H₂O was studied at 98–133 GPa, and the Py-phase was also observed to coexist with (Mg,Fe)SiO₃ (Brg and/or pPv depending on the pressure) upon laser heating (Fig. 2). These results confirm that in the presence of H₂O, the Py-phase would replace Fp to become an important constituent of the DLM. The dry reaction assemblage,



is replaced by the wet mineral assemblage in the presence of water:

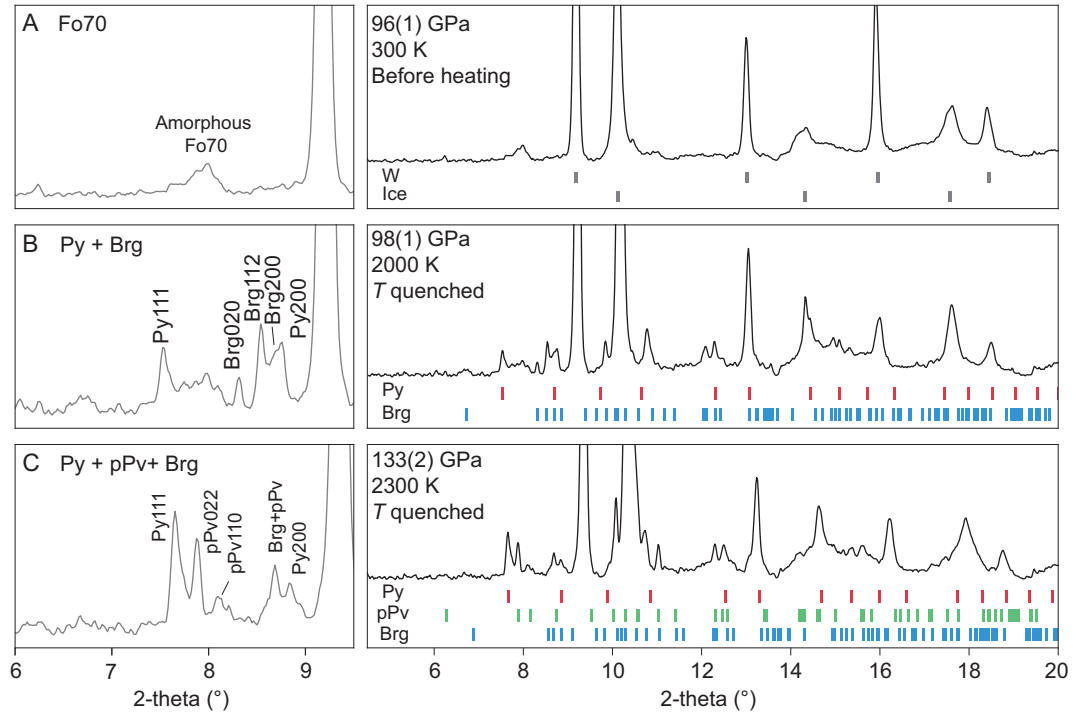
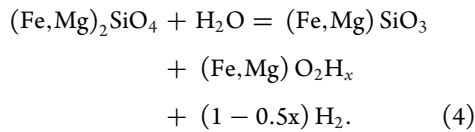
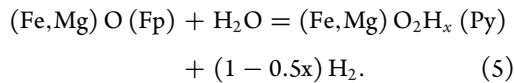


Figure 2. Py-phase synthesized from iron-bearing olivine (Fo70) and water. Left panels zoomed in for signature of high *d*-spacing peaks. (A) Amorphous Fo70 and H₂O at 96 GPa before laser heating. Strong peaks are from tungsten and ice. (B) Temperature quenched from 2000 K. New sets of diffraction peaks are associated with the Py-phase and Brg. (C) Sample was compressed to 133 GPa and heated at 2300 K. The products are Py-phase and (Mg,Fe)SiO₃ post-perovskite [3]. The X-ray wavelength was 0.3344 Å. Py, Py-phase. Brg, bridgmanite. pPv, post-perovskite type (Mg,Fe)SiO₃.



We proceeded to investigate the *P-T* dependence of the Mg fraction $X_{\text{Mg}} = \text{Mg}/(\text{Fe}+\text{Mg})$, and hydrogen content *x* in the wet assemblage. We note that the water in Eq. (4) mainly affects the silica-free oxides. The study can thus be simplified to the silica-free Fe-Mg-O-H system of the Fp to Py-phase conversion by substituting Eq. (3) into Eq. (4):



Thus, we studied the effects of water on the high-pressure chemistry of Fp. As the most abundant oxide in the mantle, Fp has been extensively investigated for its elastic, optical, thermal and elemental partitioning properties to understand the geophysical and geochemical behavior of the lower mantle (e.g. [21,22]). As a result of the very strong partitioning of Mg in Brg relative to Fp, we chose three starting Fp compositions with $X_{\text{Mg}} = 80\%$ (Pe80), 70% (Pe70) and 60% (Pe60), which would be in equilibrium with Brg of $X_{\text{Mg}} = 96\%$, 92% and

88% [23,24], respectively, in representative pyrolite compositions with bulk X_{Mg} of 90–80%. The Pe70 sample was compressed in H₂O to 96 GPa and laser-heated to 1460 K. Its XRD patterns clearly show co-existence of body-centered cubic ice-VII [17] and face-centered cubic Fp (Fig. 3A). Above 103 GPa and 1800 K, Eq. (5) proceeds to the right and the Fp-(Mg_{0.7}Fe_{0.3})O sample reacted with H₂O to form Py-(Mg_{0.7}Fe_{0.3})O₂H_x (Fig. 3B). The Py-phase is quenchable to RT under pressure (Fig. 3C). Releasing pressure at RT, the Py-phase was preserved metastable down to 50 GPa, and is unstable at lower pressures (Supplementary Figs S1 and S2). A similar transition to the Py-phase was observed with Pe60 as the starting material (Fig. 4), but the transition pressure was ~20 GPa lower than that of Pe70. The transition was not observed in the experiment with Pe80 up to 110 GPa and 2450 K, where Pe80 remained in the ferropiclsate phase without the Py-phase.

We performed conclusive crystallographic analysis on the Py-phase using a multigrain algorithm [25,26]. The algorithm picked up 10 single-crystal grains from the quenched Py-(Mg_{0.6}Fe_{0.4})O₂H_x sample after laser heating at 83.5 GPa and unambiguously indexed each single crystal to the Py-phase cubic lattice of the *Pa* $\bar{3}$ space group with its own individual orientation matrix. The crystallographic

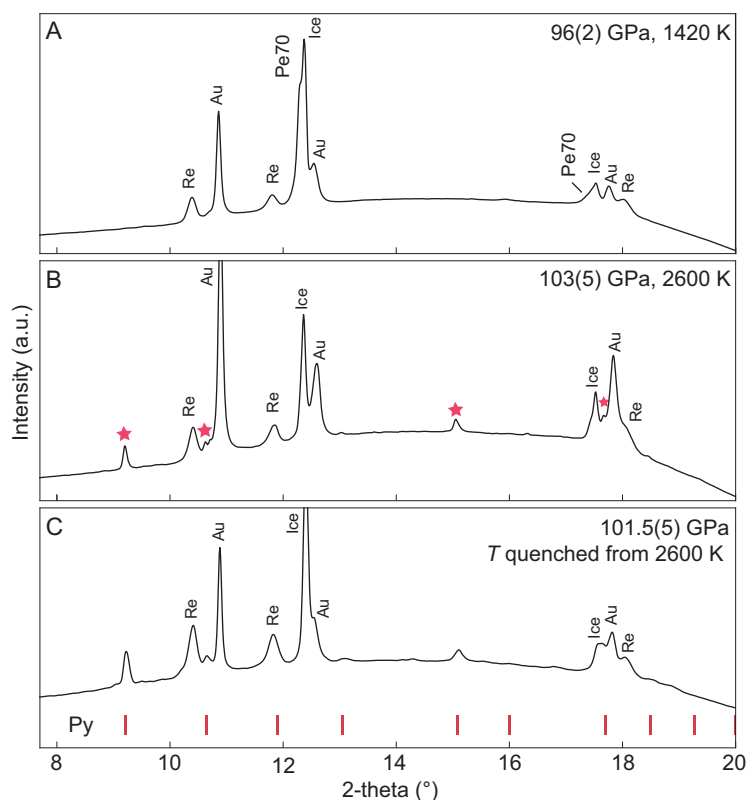


Figure 3. Py-phase synthesized from Pe70 and H₂O. (A) *In situ* X-ray diffraction pattern of Pe70+H₂O at 96 GPa and 1420 K. (B) Same as (A) but at 103 GPa and 2600 K. Peaks labeled by stars are from the Py-phase. (C) Same as (A) but at 101.5 GPa after quenching to RT. Red hash marks indicate peaks from the Py-phase. The X-ray wavelength was 0.4066 Å. We estimate ±200 K error in temperature. Py, Py-phase.

data are presented in Supplementary Tables S1 and S2. The redundant measurements yield accurate determination of lattice parameter, $a = 4.4403(16)$ Å, and volume per formula unit (f.u.), $V = 21.877(24)$ Å³, for the Py-(Mg_{0.6}Fe_{0.4})O₂H_x at 83.5 GPa and RT.

The unit-cell volume per f.u. of Py-(Mg,Fe)O₂ is a function of P - T - X_{Mg} - x (Fig. 5A). To identify the effects of different variables, we conducted an additional H-free high P - T experiment of (Mg_{0.6}Fe_{0.4})O sample loaded in pure O₂ medium without any water. We successfully synthesized H-free Py-(Mg_{0.6}Fe_{0.4})O₂ at 84 GPa, and after quenching to RT, determined its volume per f.u. to be 20.127(6) Å³ (Fig. 5A). Based on the starting composition and reported volume [10] of Mg-free Py-FeO₂ as 20.304 Å³, the volume dependence of H-free Py-(Mg,Fe)O₂ on X_{Mg} at 84 GPa and RT is represented by the linear relationship:

$$V_{Py} (\text{Å}^3) = 20.304 (1 - 0.015X_{Mg}), \quad (6)$$

where $0 < X_{Mg} < 1$. The hydrogen content x can be estimated by comparing the molar volumes of hydrogen-bearing and hydrogen-free Py-phases

of the same X_{Mg} . Following the scheme [9] used for FeO₂H_x, hydrogen content x in (Mg,Fe)O₂H_x synthesized at 83.5 GPa is estimated to be between 0.6 and 0.8 (Fig. 5A).

We further examined the cation composition of the recovered sample after complete decompression to ambient pressure. A recovered Py-(Mg_{0.6}Fe_{0.4})O₂H_x sample was analyzed using an electron microprobe (Supplementary Fig. S3). Although the sample possibly lost hydrogen and excess oxygen at ambient conditions, the overall surface Mg to (Mg+Fe) ratio (X_{Mg}) remained uniform at 0.59 ± 0.04 , indicating preservation of the cation composition during the conversion of Fp to Py-(Mg, Fe)O₂H_x.

IMPLICATIONS

Our high P - T experiments on the phase relations of Pe60, Pe70 and Pe80 are summarized in Fig. 5B, a projection of Fe-Mg-O-H quaternary phase diagram. The results clearly demonstrate that extensive solid solutions can be formed in Py-(Fe,Mg)O₂H_x, and the maximum Mg limit increases with increasing P . The results indicate that for a wet pyrolite with an average bulk composition of $X_{Mg} = 85\%$, its Fp (Pe70) will transform to the Py-phase at depths of 2100–2300 km depending upon the hot or cold geotherm temperatures [27]. For an iron-rich bulk pyrolite $X_{Mg} = 80\%$, its Fp (Pe60) will transform to the Py-phase at 1700–1900 km depth, while for an iron-poor bulk $X_{Mg} = 90\%$, its Fp (Pe80) may remain stable down to the CMB at 2891 km depth. Nevertheless, with essentially inexhaustible iron from the core, reaction (1) will kick in at the CMB to provide sufficient FeO₂H_x endmember to stabilize (Fe,Mg)O₂H_x.

As a result of the ubiquitous presence of Fp in the lower mantle, its transition to the Py-(Mg, Fe)O₂H_x carries great geological significance. Our experiments suggest that the mineralogical heterogeneity of the deep lower mantle depends upon wet or dry conditions (Fig. 6). How much water (carried by hydrous materials or as free solid or liquid H₂O) is available in the DLM remains an open question [8,28]. This relies heavily on the primordial water reservoirs and distributions [29] in the DLM as well as water circulation from the MTZ [19,30]. Previous views of a dry lower mantle were largely caused by a lack of hydrous phases that could carry water under high P - T conditions beyond the MTZ. Since the discoveries of the dense hydrous phase-H [20] and δ -AlOOH [31], hydration of the lower mantle has become an increasingly more likely scenario, which has been further strengthened by a series of subsequent observations of high P - T hydrogen-bearing phases [11,32–34]. In addition, the breakdown

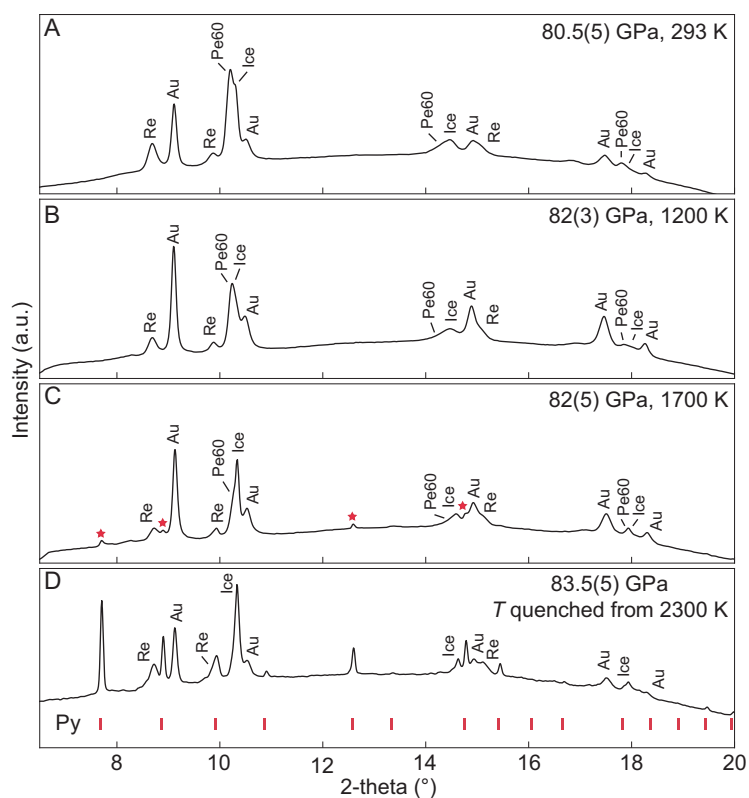


Figure 4. Py-phase synthesized from Pe60 in H₂O. *In situ* X-ray diffraction patterns were collected at the center of laser heating spot. Pe60+H₂O at 80.5 GPa and ambient temperature (A), at 82 GPa and 1200 K (B), and at 82 GPa and 1700 K (C). Stars indicate peaks from the Py-phase. (D) Same as (A) but at 83.5 GPa after quenching back to ambient temperature with red hash marks noting the Py-phase. Uncertainties in pressure were estimated from measurement error and the thermal expansion of high *P-T* gold [41]. The X-ray wavelength was 0.3445 Å. Temperature uncertainty is ±200 K in this experiment. Py, Py-phase.

of water-bearing wadsleyite and ringwoodite to anhydrous Brg and Fp does not prohibit the descent of water; the released H₂O could be carried down as inclusions in minerals [17], trapped between grain boundaries or transferred to the newly discovered high *P-T* hydrogen-bearing phases [35].

The remarkable properties and geological implications of the iron endmember Py-FeO₂H_x have been studied extensively [5,11,32,36], and can be used as guidance for the Py-(Mg,Fe)O₂H_x solid solutions. The hydrogen released from the reaction (3) in the DLM can rise freely to sustain the water-hydrogen cycle [9]. The observed low seismic velocities of Py-FeO₂H_x have been used to interpret the seismologically observed ultralow velocity zones (ULVZs) [36]. In fact, the velocities of the iron endmember are too low and some other mantle materials must be added to match the ULVZ. Likewise, Py-(Mg,Fe)O₂H_x is expected to have low velocities, but not as low as that of the iron endmember because of the presence of Mg, thus becoming a better fit for matching ULVZs.

CONCLUSION

Both Py-(Mg,Fe)O₂H_x and Py-FeO₂H_x are nominally oxygen excess phases, which are defined as the total oxygen exceeding the balance of the cations based on the ‘normal’ maximum valence state assignment of Mg²⁺, Fe³⁺, H⁺ and O²⁻. These phases could create highly inhomogeneous and unusual redox environments in the DLM [37], collect into oxygen-rich reservoirs and potentially provide a huge internal source of oxygen [10] for modulating oxygen fluctuations in the atmosphere [38,39]. Our experiments indicate that the Py-type phases cannot retain all excess oxygen after releasing pressure, thus preventing direct recovery from natural samples. They may convert to low-pressure phases with the maximum valence state, and reveal the oxidation history. This provides an alternative explanation for the high ferric inclusions often observed in natural diamonds [37,40]. In conclusion, the presence of water in DLM will create a very different mineralogy enriched in Py-(Mg,Fe)O₂H_x that has a profound impact on the evolution and dynamics of the solid Earth.

METHODS

Sample synthesis and characterization

Hydrous wadsleyite

Hydrous wadsleyite samples were synthesized with a Kawai-type 1500-ton multi-anvil apparatus at the Center for High Pressure Science and Technology Advanced Research (HPSTAR). The reaction precursors were mixed in the optimized molar ratio (0.4 FeO:1.6 Mg(OH)₂:1.0 SiO₂) and then placed in an alloy capsule made of 75% Au and 25% Pd. The Fo80 samples were synthesized at 16 GPa and heated at 1400°C for 4 hours. After samples were quenched and decompressed, the recovered samples were checked on the synchrotron beamline by XRD to be single phase wadsleyite (Fig. 1). The water content was measured from infrared-red spectroscopy and determined to be 2.2±0.3 wt% (details in Supplementary Fig. S4).

Olivine (Fo70)

Fo70 sample was synthesized at HPSTAR. The starting materials consisted of reagent grade MgO, Fe₂O₃ and SiO₂ in the proper ratio. They were loaded into separate crucibles and placed in an oven at 1600°C for more than 8 hours. After mixing well, synthesis was performed in a gas-mixing furnace for >2 hours at 1300°C and oxygen fugacity buffer of Fayalite-Magnetite-Quartz -1.

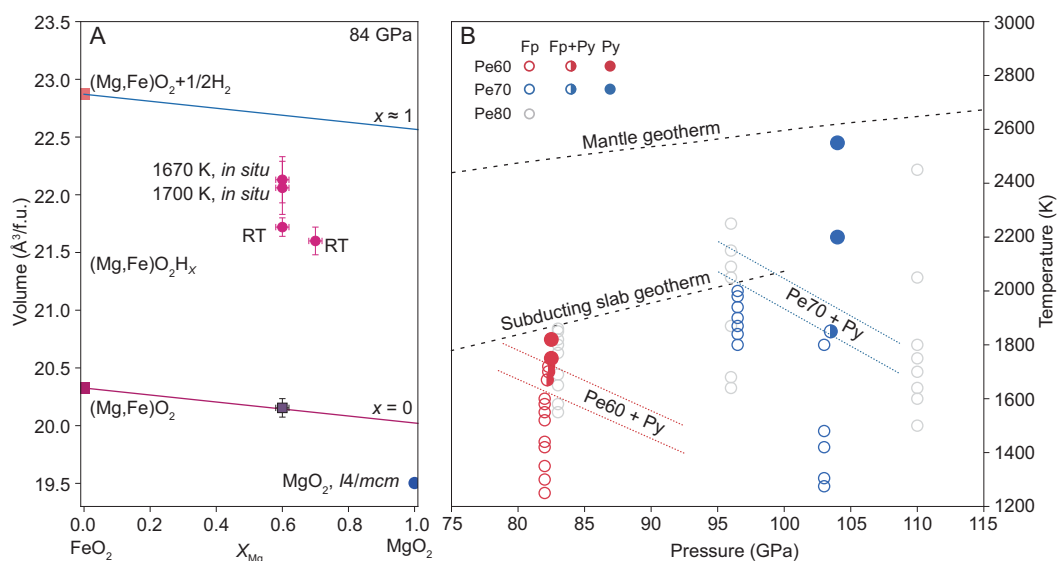


Figure 5. *P-T* phase relations for ferropericlasite with H₂O. (A) Projected *V*-*X*_{Mg} relation at 84 GPa. The Py-MgO₂ endmember is 2.6% higher in volume than the stable *I4/mcm* phase (the blue dot) [44]. Volume of (Mg_{0.7}, Fe_{0.3})O was decompressed from higher pressure to 84 GPa. f.u., formula unit. (B) Open and filled circles represent the observations of only Fp phase or the Py-phase, respectively. Half-filled circles indicate the coexistence of Fp and Py-phase. Volumes of phase-I hydrogen are from Ref. [45]. Pressure has uncertainty up to ±6 GPa at 104 GPa and 2550 K (see Methods). The uncertainty in laser heating temperature is ±200 K.

Ferropericlasite (Mg_{0.7}Fe_{0.3})O and (Mg_{0.6}Fe_{0.4})O

We synthesized ferropericlasite and olivine samples using the piston-cylinder apparatus. Fp compositions were synthesized at the Geophysical Laboratory, Carnegie Institution of Washington. MgO and

Fe₂O₃ powders were mixed according to the target mole ratio of Mg and Fe. The mixture was placed in a platinum crucible and kept in a furnace at 1300°C for 24 hours for dehydration. A solid solution of cubic (Mg,Fe)O was synthesized from the mixture of oxides at 1 GPa and 1200°C in a piston-cylinder press using a graphite capsule, which reduced ferric to ferrous iron. The composition and homogeneity of the synthesized samples were confirmed by electron probe microanalysis (Supplementary Fig. S5).

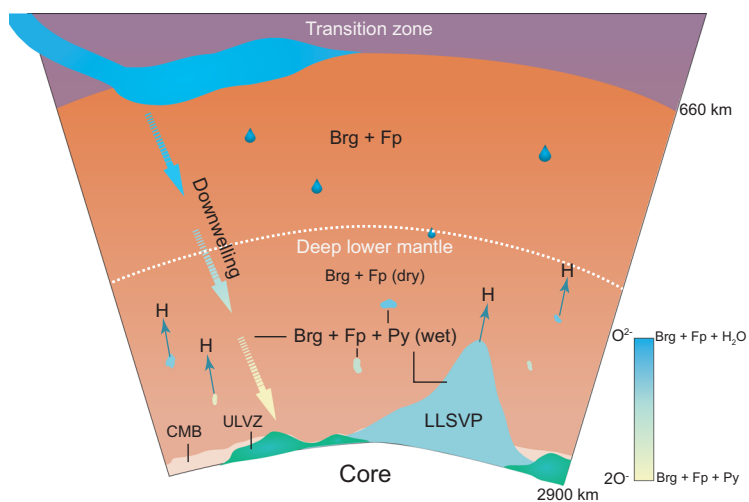


Figure 6. Mineralogy at the lower mantle. The lower mantle is divided roughly in the middle of the lower mantle, below which is the DLM. While H₂O or dense hydrous phases (blue droplets) are carried down by plate subduction or form from primitive water in shallower lower mantle, they react with Fp to form the Py-phases in the DLM (solid patches). Color gradient in the patches indicates the content of Py-phases. The mineral composition within the wet pockets of the DLM may include Brg, Fp as well as Py-(Mg, Fe)O₂H_x.

In situ XRD experiments at high *P-T* conditions

Angular dispersive XRD experiments were performed at sectors 16ID-B of HPCAT and 13ID-D of GSECARS at the APS, ANL. The x-ray energy was 30.5 keV for the samples of Pe70 in H₂O, Pe60 in O₂, 36.0 keV for Pe60 in water and 37.0 keV for Fo70 in water. Samples were pre-compressed in a pair of 1 mm diamond anvils and sample platelets of ~30 (W) × 30 (L) × 10 (T) μm³ were loaded into DACs. High pressure was achieved using beveled diamond anvils with 300 μm outer diameter and 150 or 100 μm inner diameter culet. The sample chamber was a hole of one-third of the inner culet diameter, which was drilled in a tungsten or rhenium gasket. For the experiments with H₂O, a droplet of deionized water was injected into the chamber and then was immediately sealed. For Fp+O₂ experiment, liquefied O₂ was piped into the sample chamber in a liquid-nitrogen cooled container.

One to two pieces of thin gold foil were placed around the sample as pressure calibrant. Combining the uncertainties from indexing (± 0.3 GPa) and calibrant (± 1.0 GPa), the total pressure uncertainties propagated to ± 1.1 GPa. During *in situ* laser heating, thermal pressure was corrected for thermal effects using a *P-V-T* equation of states of gold [41] and uncertainty was up to ± 6 GPa.

The diameter of laser spot at GSECARS was around 20 μm and flat down to ~ 10 μm . At the time of experiment, the incident X-ray beam size was 3×4 μm^2 . We estimated temperature uncertainties during laser heating were up to ± 200 K.

At HPCAT, the heating temperature was measured by fitting the gray-body radiation curve on both sides of the sample. The diameter of laser spot was approximately 30 μm at 2000 K, which covered the entire sample. We estimated an uncertainty of up to ± 200 K on temperature measurements throughout the laser heating experiments [42,43].

SUPPLEMENTARY DATA

Supplementary data are available at [NSR](#) online.

ACKNOWLEDGEMENTS

We thank Li Zhang for providing the Pe60 sample. We acknowledge Yingwei Fei, Neil Bennett, Jiuxing Xia, Huiyang Gou, Renbiao Tao and Colin Jackson for their help in synthesizing Pe70 in a piston-cylinder; Dale Burns, John Armstrong and Paul Goldey for assistance with scanning electronic microscopy (SEM) imaging; Liuxiang Yang for assistance in preparing samples; Tim Strobel, Haidong Zhang and Qianqian Wang for XRD screening after sample synthesis. XRD measurements were performed at 16ID-B sector of High Pressure Collaborative Access Team (HPCAT) and 13ID-D sector of GeoSoilEnviroCARS (GSECARS), Advanced Photon Source (APS), Argonne National Laboratory (ANL). Infrared-red spectroscopy was performed at Zhejiang University.

FUNDING

This work is supported by the National Natural Science Foundation of China (U1530402, U1930401 and 17N1051-0213). HKM is supported by the National Science Foundation of the US (NSF) (EAR-1722515 and EAR-1447438). JL, WM and JC acknowledge support from the NSF Geophysics Program (EAR 1446969 and EAR 1723185). HPCAT operations are supported by DOE-NNSA's Office of Experimental Sciences. GSECARS is supported by the NSF (EAR 1634415) and DOE-GeoSciences (DE-FG02-94ER14466). APS is supported by DOE-BES, under contract no. DE-AC02-06CH11357.

AUTHOR CONTRIBUTIONS

H.-K.M., Q.H., J.L. and W.L.M conceived the project. Q.H., J.L., Y. M. and V.B.P. performed experiments. J.C. and B.Y. grew the hydrous wadsleyite crystals. Q.H. and J.L. analyzed the data.

Q.H., J.L. and H.-K. M. wrote the manuscript with input from all authors.

Conflict of interest statement. None declared.

REFERENCES

1. Tschauner O, Ma C and Beckett JR *et al.* Discovery of bridgmanite, the most abundant mineral in Earth, in a shocked meteorite. *Science* 2014; **346**: 1100–2.
2. Badro J, Fiquet G and Guyot F *et al.* Iron partitioning in Earth's mantle: toward a deep lower mantle discontinuity. *Science* 2003; **300**: 789–91.
3. Murakami M, Hirose K and Kawamura K *et al.* Post-perovskite phase transition in MgSiO_3 . *Science* 2004; **304**: 855–8.
4. Duffy T. Crystallography's journey to the deep Earth. *Nature* 2014; **506**: 427–9.
5. Liu J, Hu Q and Bi W *et al.* Altered chemistry of oxygen and iron under deep Earth conditions. *Nat Commun* 2019; **10**: 153.
6. Boulard E, Harmand M and Guyot F *et al.* Ferrous iron under oxygen-rich conditions in the deep mantle. *Geophys Res Lett* 2019; **46**: 1348–56.
7. Mao H-K and Mao WL. Key problems of the four-dimensional Earth system. *Matter Radiat Extremes* 2020; **5**: 038102.
8. Ni H, Zheng Y-F and Mao Z *et al.* Distribution, cycling and impact of water in the Earth's interior. *Natl Sci Rev* 2017; **4**: 879–91.
9. Hu Q, Kim DY and Liu J *et al.* Dehydrogenation of goethite at lower mantle condition. *Proc Natl Acad Sci USA* 2017; **114**: 1498–501.
10. Hu Q, Kim DY and Yang W *et al.* FeO_2 and FeOOH under deep lower-mantle conditions and Earth's oxygen–hydrogen cycles. *Nature* 2016; **534**: 241–4.
11. Boulard E, Guyot F and Menguy N *et al.* CO_2 -induced destabilization of pyrite-structured FeO_2Hx in the lower mantle. *Natl Sci Rev* 2018; **5**: 870–7.
12. Nishi M, Kuwayama Y and Tsuchiya J *et al.* The pyrite-type high-pressure form of FeOOH . *Nature* 2017; **547**: 205–8.
13. Yamanaka T, Kyono A and Nakamoto Y *et al.* New structure of high-pressure body-centered orthorhombic Fe_2SiO_4 . *Am Mineral* 2015; **100**: 1736–43.
14. Smyth J. The β - Mg_2SiO_4 : a potential host for water in the mantle? *Am Mineral* 1987; **72**: 1051–5.
15. Pearson DG, Brenker FE and Nestola F *et al.* Hydrous mantle transition zone indicated by ringwoodite included within diamond. *Nature* 2014; **507**: 221–4.
16. Schmandt B, Jacobsen SD and Becker TW *et al.* Dehydration melting at the top of the lower mantle. *Science* 2014; **344**: 1265–8.
17. Tschauner O, Huang S and Greenberg E *et al.* Ice-VII inclusions in diamonds: evidence for aqueous fluid in Earth's deep mantle. *Science* 2018; **359**: 1136–9.
18. Ohtani E. The role of water in Earth's mantle. *Natl Sci Rev* 2020; **7**: 224–32.
19. Lin Y, Hu Q and Meng Y *et al.* Evidence for the stability of ultra-hydrous stishovite in Earth's lower mantle. *Proc Natl Acad Sci USA* 2020; **117**: 184–9.

20. Nishi M, Irifune T and Tsuchiya J *et al.* Stability of hydrous silicate at high pressures and water transport to the deep lower mantle. *Nat Geosci* 2014; **7**: 224–7.
21. Wu Z and Wentzcovitch RM. Spin crossover in ferropericlase and velocity heterogeneities in the lower mantle. *Proc Natl Acad Sci USA* 2014; **111**: 10468–72.
22. Antonangeli D, Siebert J and Aracne CM *et al.* Spin crossover in ferropericlase at high pressure: a seismologically transparent transition? *Science* 2011; **331**: 64–7.
23. Sinmyo R, Hirose K and Nishio-Hamane D *et al.* Partitioning of iron between perovskite/postperovskite and ferropericlase in the lower mantle. *J Geophys Res Solid Earth* 2008; **113**: B11204.
24. Mao H-K, Shen G and Hemley RJ. Multivariable dependence of Fe-Mg partitioning in the lower mantle. *Science* 1997; **278**: 2098–100.
25. Sørensen HO, Schmidt S and Wright JP *et al.* Multigrain crystallography. *Z Kristallogr* 2012; **227**: 63–78.
26. Zhang L, Yuan H and Meng Y *et al.* Development of high-pressure multigrain X-ray diffraction for exploring the Earth's interior. *Engineering* 2019; **5**: 441–7.
27. Katsura T, Yoneda A and Yamazaki D *et al.* Adiabatic temperature profile in the mantle. *Phys Earth Planet Inter* 2010; **183**: 212–8.
28. Yang X, Liu D and Xia Q. CO₂-induced small water solubility in olivine and implications for properties of the shallow mantle. *Earth Planet Sci Lett* 2014; **403**: 37–47.
29. Hallis LJ, Huss GR and Nagashima K *et al.* Evidence for primordial water in Earth's deep mantle. *Science* 2015; **350**: 795–7.
30. Ni H, Zhang L and Guo X. Water and partial melting of Earth's mantle. *Sci China Earth Sci* 2016; **59**: 720–30.
31. Pamato MG, Myhill R and Boffa Ballaran T *et al.* Lower-mantle water reservoir implied by the extreme stability of a hydrous aluminosilicate. *Nat Geosci* 2014; **8**: 75–9.
32. Yuan L, Ohtani E and Ikuta D *et al.* Chemical reactions between Fe and H₂O up to megabar pressures and implications for water storage in the Earth's mantle and core. *Geophys Res Lett* 2018; **45**: 1330–8.
33. Zhang L, Yuan H and Meng Y *et al.* Discovery of a hexagonal ultradense hydrous phase in (Fe,Al)OOH. *Proc Natl Acad Sci USA* 2018; **115**: 2908–11.
34. Zhu S-C, Hu Q and Mao WL *et al.* Hydrogen-bond symmetrization breakdown and dehydrogenation mechanism of FeO₂H at high pressure. *J Am Chem Soc* 2017; **139**: 12129–32.
35. Iizuka-Oku R, Yagi T and Gotou H *et al.* Hydrogenation of iron in the early stage of Earth's evolution. *Nat Commun* 2017; **8**: 14096.
36. Liu J, Hu Q and Kim DY *et al.* Hydrogen-bearing iron peroxide and the origin of ultralow-velocity zones. *Nature* 2017; **551**: 494–7.
37. Stagno V, Ojwang DO and McCammon CA *et al.* The oxidation state of the mantle and the extraction of carbon from Earth's interior. *Nature* 2013; **493**: 84–8.
38. Lyons TW, Reinhard CT and Planavsky NJ. The rise of oxygen in Earth's early ocean and atmosphere. *Nature* 2014; **506**: 307–15.
39. Edwards CT, Saltzman MR and Royer DL *et al.* Oxygenation as a driver of the Great Ordovician Biodiversification Event. *Nat Geosci* 2017; **10**: 925–9.
40. Palot M, Jacobsen SD and Townsend JP *et al.* Evidence for H₂O-bearing fluids in the lower mantle from diamond inclusion. *Lithos* 2016; **265**: 237–43.
41. Anderson OL, Isaak DG and Yamamoto S. Anharmonicity and the equation of state for gold. *J Appl Phys* 1989; **65**: 1534–43.
42. Meng Y, Hrubiak R and Rod E *et al.* New developments in laser-heated diamond anvil cell with in-situ x-ray diffraction at High Pressure Collaborative Access Team. *Rev Sci Instrum* 2015; **86**: 072201.
43. Prakashenka VB, Kubo A and Kuznetsov A *et al.* Advanced flat top laser heating system for high pressure research at GSECARS: application to the melting behavior of germanium. *High Pressure Res* 2008; **28**: 225–35.
44. Lobanov SS, Zhu Q and Holtgrewe N *et al.* Stable magnesium peroxide at high pressure. *Sci Rep* 2015; **5**: 13582.
45. Ji C, Li B and Liu W *et al.* Crystallography of low Z material at ultrahigh pressure: case study on solid hydrogen. *Matter Radiat Extremes* 2020; **5**: 038401.